



Universiteit
Leiden
The Netherlands

Identification and characterization of novel factors in the DNA damage response

Singh, J.K.

Citation

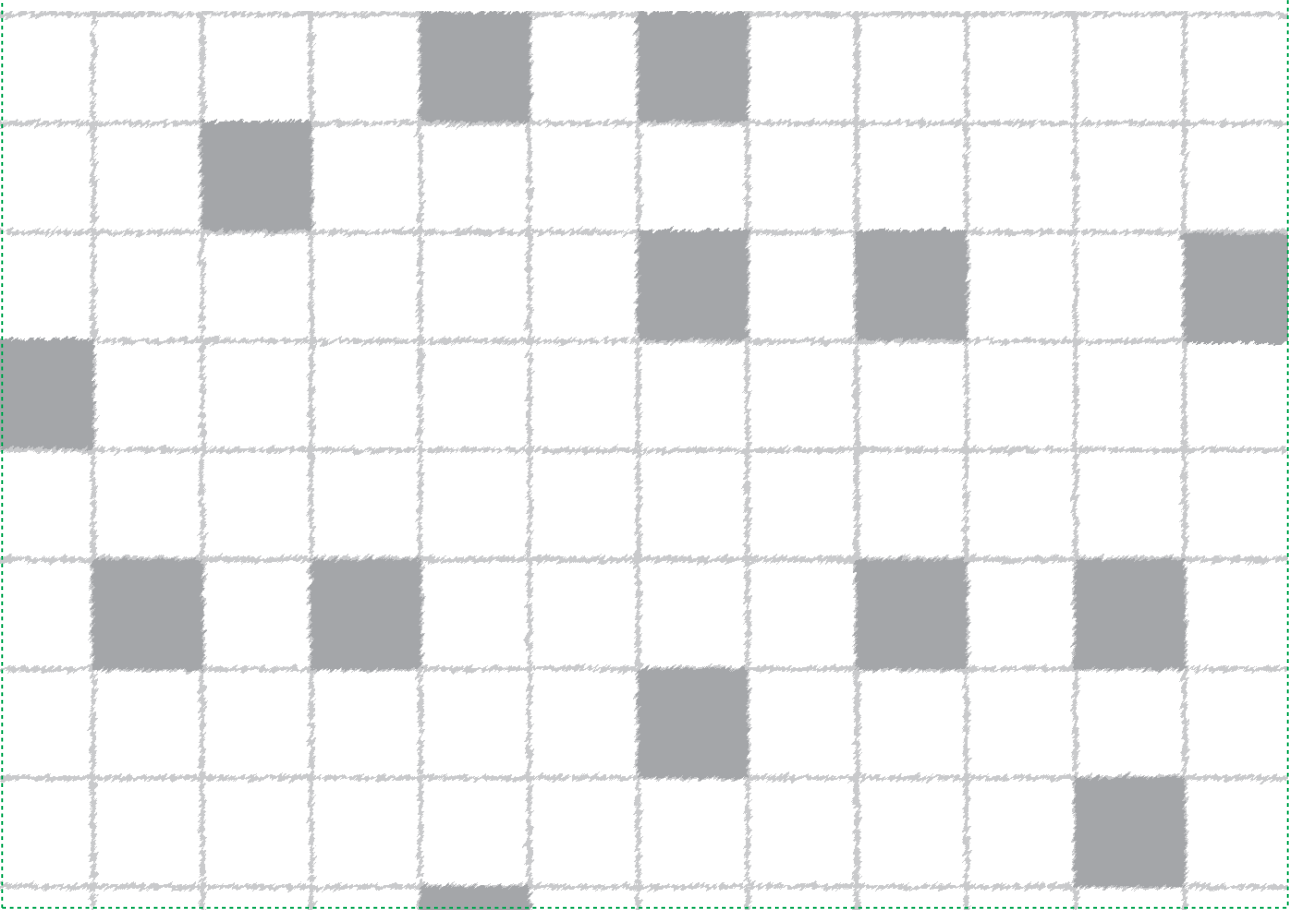
Singh, J. K. (2022, November 9). *Identification and characterization of novel factors in the DNA damage response*. Retrieved from <https://hdl.handle.net/1887/3485639>

Version: Publisher's Version

License: [Licence agreement concerning inclusion of doctoral thesis in the Institutional Repository of the University of Leiden](#)

Downloaded from: <https://hdl.handle.net/1887/3485639>

Note: To cite this publication please use the final published version (if applicable).



CHAPTER 4

KANSL3 suppresses R-loop formation and replication fork instability

Jenny Kaur Singh, Jolanthe Lingeman, Wouter W. Wiegant, Anton J.L. de Groot, Román González-Prieto, Alfred C.O. Vertegaal, and Haico van Attikum

ABSTRACT

KANSL3 is a member of the NSL chromatin remodeling complex. This complex is mainly involved in the transcriptional regulation of housekeeping genes. Whether this complex plays a role in processes other than transcription is largely unclear. Here we show that KANSL3 is a novel factor involved in the replication stress response. We found that KANSL3-depleted cells display an increased sensitivity to hydroxyurea. Furthermore, we observed that after hydroxyurea treatment, KANSL3-depleted cells show increased pRPA levels, reduced fork restart as measured by DNA fiber analysis and increased R-loop formation. Interestingly, increased levels of pRPA and R-loops were also observed in untreated cells. These results suggest that KANSL3 has a suppressive role on R-loop formation, thereby preventing collisions between the replication fork and the transcription machinery that can lead to replication fork arrest/collapse. How KANSL3's role in transcription regulation affects R-loop formation and consequently replication fork stability/recovery following stress is subject of future studies.

Keywords: Replication stress (RS), R-loops, KANSL3, NSL complex

INTRODUCTION

DNA replication is a tightly regulated process that guarantees the accurate duplication of the genome once per cell cycle. DNA replication is, however, constantly challenged by several sources, which can cause a phenomenon known as replication stress (RS) [1]. RS is defined as the slowing or stalling of replication fork progression and/or DNA synthesis, and can be caused by for instance limiting nucleotides, ribonucleotide incorporation, repetitive DNA elements, transcription-replication conflicts, DNA secondary structures, fragile sites, and oncogene-induced stress [2]. Fortunately, cells have evolved sophisticated S phase and mitotic checkpoint pathways that help DNA replication to complete in the face of RS. Defects in these checkpoint pathways can lead to the stalling or collapse of replication forks, which in turn can cause mutations, chromosome rearrangements or the missegregation of chromosomes, thereby contributing to the development of diseases such as cancer [1].

ATR is the major kinase involved in dealing with RS and is recruited to RPA-coated single-stranded DNA (ssDNA) generated by uncoupling of the replicative MCM helicase from DNA polymerases during replication fork stalling [3]. This is followed by the ATR activation via two parallel pathways mediated by either ETAA1 or TOPBP1. ETAA1 stimulates ATR signaling by binding RPA on ssDNA, whereas TOPBP1 does so via its interaction with the RAD17 and 9-1-1 complexes at single-strand/double-strand DNA junctions [4, 5]. Once activated, ATR phosphorylates a wide variety of substrates, including CHK1 [6]. ATR-CHK1 then promote the restart of stalled replication forks, which may e.g. have arisen by uncoupling of the replicative MCM helicase from DNA polymerases, while enabling the slowdown or arrest of cell cycle progression until replication is completed [2], and controlling the firing of new origins to preserve the RPA pool [3]. Another protective mechanism that ensures fork integrity is replication fork reversal. During this process, the nascent DNA strands on each sister chromatid are reannealed to form a fourth regressed arm, which becomes actively converted into a Holliday junction (HJ)-like structure [7]. Several key players are involved in fork reversal such as the SWI/SNF chromatin remodelers SMARCAL1 and ZRANB3, as well as the helicase HLTf [8]. Reversed forks are substrates for degradation by the nuclease MRE11 and must be properly protected by BRCA1, BRCA2 and Fanconi anemia (FA) proteins FANCA, FANCD2 and FANCI to prevent fork collapse and ensure fork restart [9]. Alternatively, replication forks that stall at DNA lesions can restart downstream of the lesion by PrimPol-dependent re-priming on the leading strand, leaving unreplicated

ssDNA gaps to be filled post-replicatively by translesion synthesis (TLS) polymerases such as POL η and REV1, or by template switching (TS), during which an undamaged homologous template on the sister chromatid is used to bypass DNA lesions [10].

Given the fact that DNA replication and transcription both utilize DNA, it is unavoidable that the two processes will interfere with each other, giving rise to transcription-replication conflicts (TRCs) [2]. TRCs can occur in a head-on (HO) or co-directional orientation (CD), depending on the orientation of the genes relative to the replication fork directionality. In mammalian cells the majority of replication forks progress through genes in a CD orientation to avoid the more deleterious HO collisions [11]. TRCs that occur in an HO orientation are frequently associated with the formation and persistence of R-loops. These are structures in which RNA is annealed to genomic DNA to create an RNA:DNA hybrid surrounded by a loop of non-templated single-stranded DNA which is protected by RPA [12, 13]. While R-Loops have several regulatory and topological roles in genome regulation, their persistence and association with TRCs can cause replication-stress associated genome instability [14]. However, although the network of R-loop regulators is expanding, a full understanding of the context in which R-loops arise and cause TRC-associated genome instability is lacking [15].

Chromatin factors have emerged as important players in R-loop formation and the associated genome instability [16]. These factors include the member of the MSL (male specific lethal) histone acetyltransferase (HAT) complex MOF, which has been reported to suppress replication fork stalling and R-loop formation [17]. Besides the MSL chromatin remodeling complex, MOF is also shared within the non-specific lethal (NSL) complex which consists of four core members KANSL1, KANSL2, KANSL3 and PHF20 [18]. The NSL complex was found to associate with the promoters of transcriptionally active genes, particularly housekeeping genes. [18], and regulates the expression of several genes essential for cell proliferation [19]. Also, more recently the loss of NSL complex members was associated with abnormalities in nuclear morphology and genome instability [20]. However, despite several studies linking the MSL and NSL chromatin remodeling complexes to transcription regulation and RS, the underlying molecular mechanism remains unclear.

Here we describe an important regulatory role of the NSL-complex member KANSL3 in the RS response. We found that KANSL3, unlike MOF, is not involved in the regulation of H4K16Ac in chromatin. KANSL3 protects cells from HU-induced RS and is implicated in the restart of stalled replication forks. We speculate that KANSL3 may suppress R-loop induced TRCs that lead to replication fork stalling and/or collapse.

RESULTS

The NSL complex member KANSL3 is dispensable for H4K16Ac levels

MOF forms the catalytic core of the NSL and MSL complex. [18]. As part of the MSL complex, MOF is the key lysine acetyltransferase (KAT) responsible for histone H4 lysine (K) 16 acetylation (H4K16Ac)-dependent decompaction of chromatin structure in mammalian cells (Fig. 1A and [20]). Since MOF is also part of the NSL complex, we asked whether this complex could also be involved in H4K16Ac. To examine this, we monitored the levels of H4K16Ac in chromatin-enriched extracts from cells depleted of the NSL complex members KANSL3 or MOF (Fig. 1A). As expected, depletion of MOF decreased the H4K16Ac levels in chromatin, while KANSL3 knockdown showed no effect (Fig. 1B). During the course of this work, several other studies also observed no change in H4K16Ac levels in KANSL3-depleted cells, suggesting distinct MSL- and NSL-complex characteristics [19, 20]. In fact, MOF acetylates lamin A/C as part of the NSL complex in order to maintain nuclear architecture [20]. Moreover, MOF induces H4K5Ac and H4K8Ac at transcription start sites (TSS) of genes involved in cell proliferation as part of the NSL-complex [19]. Together, our data in agreement with other studies suggests that the MSL and NSL complexes function in an H4K16Ac-dependent and -independent manner.

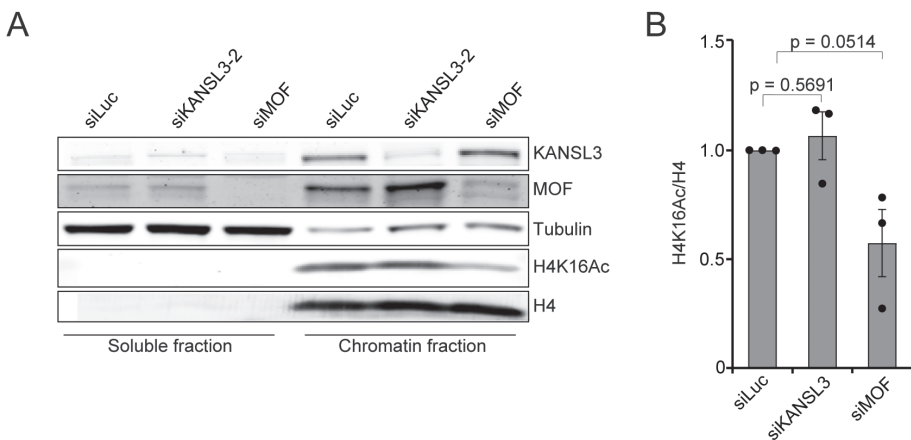


Figure 1. KANSL3 is dispensable for H4K16Ac. (A) Western blot analysis of the indicated proteins in soluble and chromatin fractions from U2OS cells. H4 is the loading control. A representative experiment is shown (B) Quantification of H4K16Ac levels on chromatin in cells from D. H4 is a loading control, which was used for normalization of H4K16Ac levels on chromatin. The mean \pm SEM from 3 independent experiments is shown.

KANSL3 interacts with members of the NLS and MSL complex

To further unravel how the NSL complex may operate in a manner distinct from MSL, we asked whether KANSL3 has additional interaction partners besides its members in the NSL complex. To this end, we generated U2OS Flp-In/T-Rex cells stably expressing inducible GFP-tagged KANSL3 or GFP-NLS and performed GFP-trap based pulldowns followed by label-free mass spectrometry (MS). Our analysis revealed that KANSL3 interacts with 30 proteins that were at least 2-fold enriched in GFP-KANSL3 pulldowns compared to those of GFP-NLS (Fig. S1A and Table S1). Although, most interactors were known members of the NSL and MSL complexes (e.g. KANSL1, KANSL2 and KAT8), we also found additional interaction partners including NAT10, SUPT6H, SUPT16H, SCAF1 and PARP2 (Table S1). Since KANSL3's interaction partner MOF has previously been implicated in the response to RS [17], we performed this interaction analysis also in response to hydroxyurea (HU), which induces RS by dNTP depletion (Fig. S1B and Table S1). Interestingly, we found that KANSL3 interacts with PARP2, a protein that stabilizes RAD51 at stalled replication forks [21], with subunits of the RNA polymerase II complex (e.g. POLR2A, POLR2B and POLR2E), and with factors involved in RNA splicing (e.g. SRSF1 and SCAF1). Together, these results suggest that KANSL3 may interact with proteins involved in transcription and the RS response, manifesting a possible role of the NSL complex in these processes, although these interactions need to be confirmed.

KANSL3 promotes cell survival upon replication stress

To assess whether KANSL3, similar to MOF, is implicated in the RS response [17], we performed clonogenic cell survival assays in the presence and absence of HU. We found that KANSL3 loss rendered cells sensitive to HU, an effect that was similar to that observed after depletion of RPA-interacting protein ETAA1 (Fig. 2A-B). Cell cycle profiles remained unaffected in KANSL3-depleted cells, ruling out effects of cell cycle mis-regulation (Fig. S2A). Finally, we employed the Flp-In/T-Rex system to establish HCT116 cells stably expressing inducible and siRNA-resistant GFP-tagged KANSL3 (Fig. 2C). Confirming our previous data (Fig. 2A), we found that KANSL3 knockdown rendered cells sensitive to HU. Importantly, expression of siRNA-resistant GFP-KANSL3 almost fully rescued the HU sensitivity observed after KANSL3 knockdown (Fig. 2B), ruling out off-target effects of the siRNA against KANSL3.

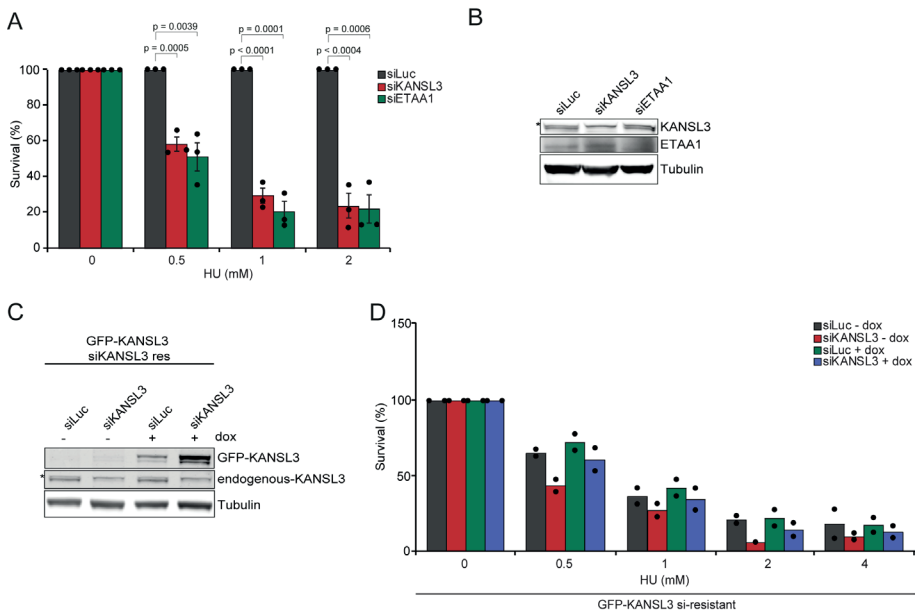


Figure 2. KANSL3-depleted cells are HU-sensitive. (A) Relative survival efficiency in HCT116 cells transfected with the indicated siRNAs and treated with 0.5, 1 and 2 mM HU. The mean \pm SEM of 3 independent experiments is shown. Data were normalized to un-irradiated conditions and set to 100%. Statistical significance was calculated using Student's *t* test. (B) Western blot analysis of the expression of endogenous KANSL3 and ETAA1 from cells in A. Tubulin is a loading control. (C) Expression levels of endogenous KANSL3 and dox-inducible siRNA-resistant GFP-KANSL3 in HCT116 Flp-In/TRex cells. Tubulin is a loading control. (D) Effect of inducible expression of GFP-NLS and siRNA resistant GFP-tagged KANSL3 on the survival of stable HCT116 Flp-In/TRex after transfection with indicated siRNAs and treatment with indicated doses of ionizing irradiation (IR). The mean of 2 independent experiments is shown. Data was normalized to siLuc control which was set to 100%. Statistical significance was calculated using the Student's *t* test.

KANSL3 does not regulate replication fork speed and replication fork protection

To better understand how the absence of KANSL3 sensitizes cells to RS, we performed DNA fiber assays to monitor DNA replication in unperturbed conditions. We monitored progression rates of individual replication forks in control and KANSL3-depleted cells. For this, we sequentially labeled cells with CldU (green) and IdU (red), which was followed by tract length analysis. In line with previous results, PARPi treated cells showed an increase in fork speed [22]. However, KANSL3 depletion did not significantly impact tract lengths when compared to that in control cells (Fig. 3A). These data suggest that KANSL3 does not affect DNA replication in unperturbed conditions.

Next, we asked whether KANSL3 plays a role in stabilizing DNA replication forks under stressed conditions. In order to study this, siRNA-transfected U2OS cells were sequentially labeled with CldU and IdU, and on-going replication forks were then stalled by HU treatment. The relative shortening of the IdU tract length upon HU treatment served as a measure for fork degradation. As expected, BRCA2 knockdown cells displayed a significant reduction in IdU tract length compared to that in control cells [23]. In contrast, KANSL3-depleted cells displayed no significant reduction in IdU tract length (Fig. 3B). This suggests that KANSL3 is not involved in protecting stalled replication forks from degradation.

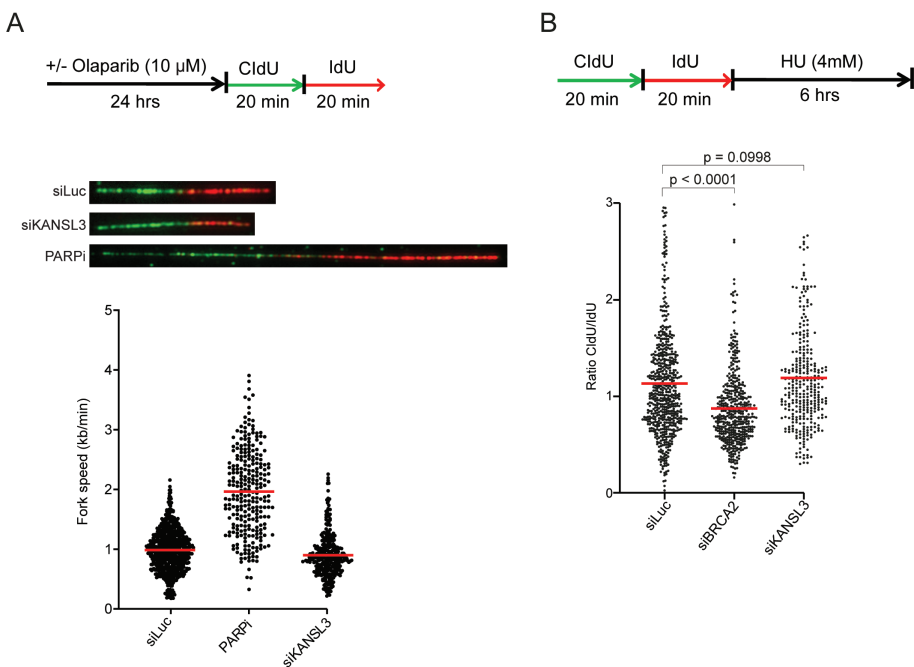


Figure 3. KANSL3 is dispensable for replication fork speed and replication fork protection. (A) DNA fiber speed analysis in U2OS cells transfected with the indicated siRNAs or treated with 10 μ M Olaparib (PARPi) for 24 hrs. Cells were labelled for 20 minutes with CldU (green), followed by labelling with IdU (red) for 20 minutes. Fork speed was calculated as labelled IdU length by pulse time. Red bars indicate the mean fork speed. Representative fibers of different conditions are shown. (B) Fork degradation analysis of siRNA transfected U2OS cells labelled as in A and treated with 4 mM HU for 6 hrs. Plotted values represent ratios of CldU versus IdU. Red bars indicate the mean fork speed. P -values were derived from Kruskal–Wallis ANOVA Dunn’s post test.

KANSL3 promotes replication fork restart following replication fork stalling

Since the loss of MOF has been attributed to S-phase progression defects, as well as impaired fork restart upon RS [17], we aimed at further substantiating our findings by unraveling whether KANSL3 is also implicated in this process. To address this, we performed an ethynyl-2'-deoxyuridine (EdU) incorporation assay in which MOF or KANSL3-depleted cells were left untreated or treated with HU to stall replication forks, followed a release in medium containing EdU to allow and monitor replication restart (Fig. 4A). We found that control cells fully recovered from the HU treatment during the course of two hours, whereas KANSL3-depleted cells displayed reduced EdU incorporation at all timepoints. Strikingly, MOF depletion did not exert any effect on EdU incorporation (Fig. 4B). To our surprise, we also found KANSL3 depletion to reduce EdU staining in unperturbed conditions (Fig. 4B). Given that KANSL3-depleted cells did not display any change in fork speed, it may be possible that the reduced EdU incorporation observed in these cells, is due to a decrease in origin firing [24]. On another note, we also found that cell cycle profiles displayed a mild increase in the fraction of KANSL3-depleted cells in the G2/M phase (Fig. S2A). This may be indicative of an increase in the levels of under-replicated DNA in KANSL3-depleted cells, which could eventually trigger a G2/M cell cycle arrest.

Next, we sought to investigate whether the decrease in EdU incorporation observed in KANSL3-depleted cells (Fig. 4B) is due to defects in the restart of stalled replication forks. To this end, we performed DNA fiber assays in which siRNA-transfected U2OS cells were labeled with CldU, treated with HU, and released into IdU. We found that HU-treated KANSL3-depleted cells, similar to RAD51-depleted cells, exhibited a decrease in the restart of stalled forks (Fig. 4C-D), the latter of which is in line with previous results [25].

To further substantiate these findings, we sought to address if KANSL3 is involved in ATR signaling following HU-induced helicase-polymerase uncoupling. ATR is the major kinase, which preserves the nuclear RPA pool by restraining the firing of new origins in order to prevent replication fork instability. Inhibition of ATR in HU-treated cells leads to excessive double-strand break (DSB) formation and RPA hyperphosphorylation [3]. Consistent with a decrease in replication fork restart likely caused by replication fork instability, KANSL3-depleted cells showed increased levels of RPA2 phosphorylation at Serine 4 and 8 (Fig. 4E-F), as well as a mild increase in γ H2AX levels (Fig. 4G). Importantly, RPA levels remained unchanged in HU-treated KANSL3-depleted cells (Fig. S2B-C), suggesting that KANSL3 loss results in the increase of stalled and collapsed replication forks upon HU-induced RS. Taken together, these results suggest that KANSL3 is important to maintain fork integrity under RS.

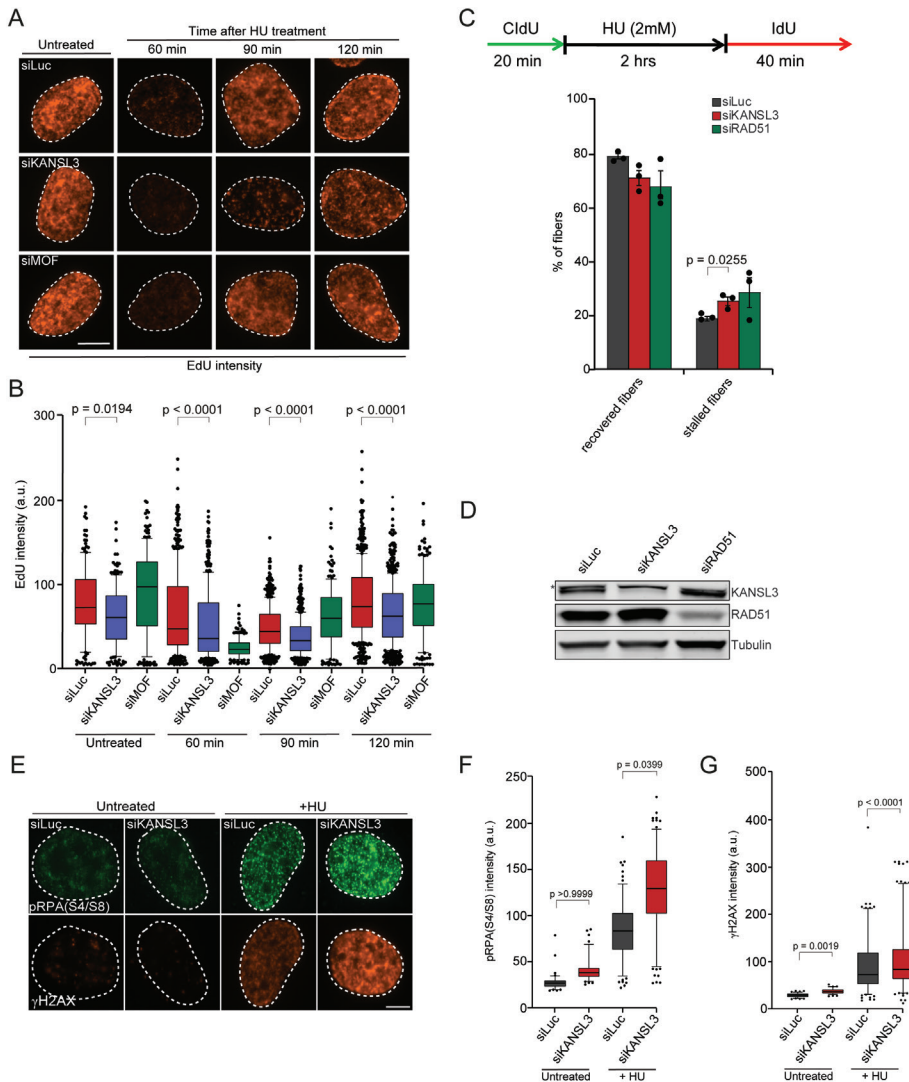


Figure 4. KANSL3 promotes recovery from HU-stalled replication forks. (A) Representative results of immunofluorescence microscopy of the BrdU incorporation assay. (B) The BrdU of individual cells in the results in A are depicted in a boxplot. P -values were derived from Kruskal–Wallis ANOVA Dunn’s post test. (C) Fork recovery analysis in U2OS cells transfected with the indicated siRNAs, followed by CldU labelling, 4 mM HU treatment for 6 hours and IdU labelling for 40 minutes. Fork progression (IdU-positive tracks) in U2OS cells transfected with the indicated siRNAs. Statistical significance was calculated using the Student’s t test. (D) Western blot analysis of the expression of endogenous KANSL3 and RAD51 from cells in C. Tubulin is a loading control. (E) Phosphorylated RPA at Ser4/8 foci formation in U2OS cells transfected with the indicated siRNAs. Cells were exposed to 2 mM of HU and foci intensity was measured after 4 hours. (F) Quantification of RPA (S4/8) foci intensity in cells from E. Mean foci intensity was quantified in immuno-stained p-RPA (S4/8) cells. The mean of 3 independent experiments is shown. (F) As in E, except that γ H2AX foci intensity was measured. Statistical significance was calculated using the Student’s t test.

KANSL3-depleted cells suffer from aberrant RNA-DNA hybrid formation

Given the role of the NSL complex in regulating transcription [26], we hypothesized that transcription-replication conflicts (TRCs) might be responsible for the observed RS in KANSL3-depleted cells. TRCs are often associated with increased levels of RNA-DNA hybrid structures (R-loops). We therefore tested the impact of KANSL3 on R-loop formation using the S9.6 antibody for immunofluorescence, which mostly recognizes R-loops, but also has low affinity for dsRNA structures [27]. In order to validate our S9.6 immunofluorescence staining, we depleted a well-known R-loop processing factor AQR and found, as expected, that this led to an increase in the R-loop levels (Fig. 5A-B and [28]). Next, we measured the accumulation of R-loops in KANSL3- or MOF-depleted cells in both undamaged and HU-treated cells. While loss of KANSL3 severely increased the accumulation of R-loops under both conditions, MOF depletion did not, the latter of which being in contrast with a previous study, (Fig. 5A-B and [17]). Together, these results suggest that KANSL3, but not MOF, is involved in suppressing R-loop formation in unperturbed and RS conditions. We speculate that KANSL3 prevents the formation of TRCs by suppressing R-loop formation and the subsequent stalling/collapse of replication forks (Fig. 5C).

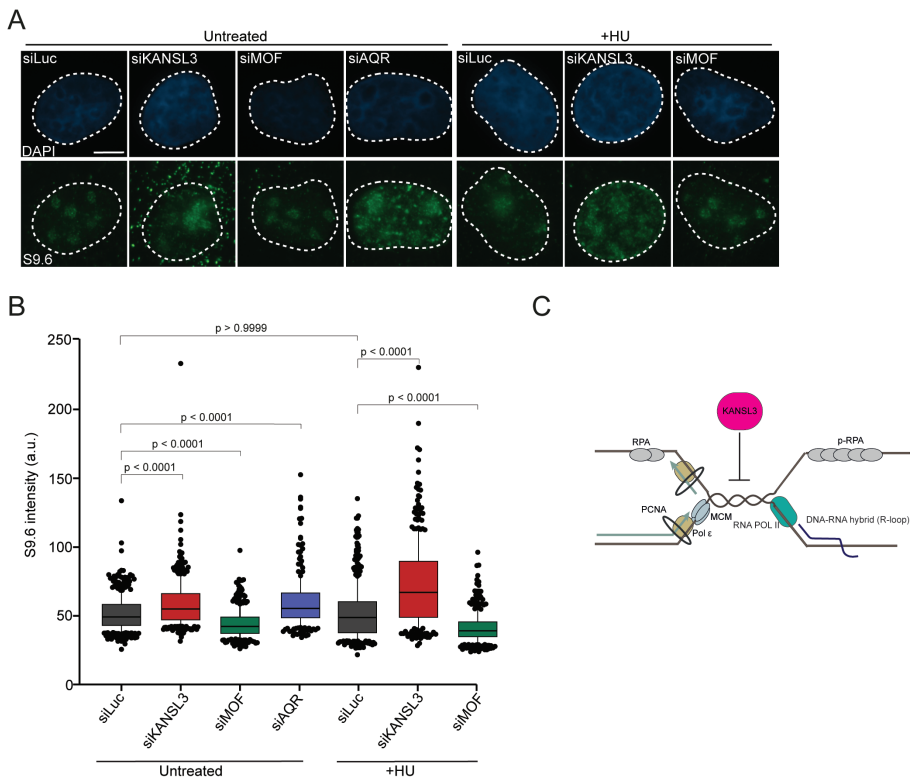


Figure 5. KANSL3 suppresses the formation of R-loops. (A) S9.6 nuclear intensity was measured in U2OS cells transfected with the indicated siRNAs. Cells were exposed to 2 mM of HU and foci intensity was measured after 4 hours. The S9.6 signal intensity per nucleus was determined by subtracting the S9.6 staining with that from nucleoli in each nucleus. (B) Quantification of S9.6 intensity in cells from A. Mean intensity was quantified in immuno-stained S9.6 cells. *P*-values were derived from Kruskal–Wallis ANOVA Dunn’s post test. (C) Model for how KANSL3 works during RS and R-loops formation. KANSL3 suppresses the formation of aberrant R-loops, thereby preventing replication fork arrest/collapse as a result collisions between ongoing replication forks and the replication machinery.

DISCUSSION

In this study, we uncover an important role of the NSL chromatin remodeling complex member KANSL3 in the RS response. First, we demonstrate that KANSL3 is not implicated in H4K16Ac formation, although it associates with both MSL and NSL complex members, including the HAT MOF, which is responsible for H4K16Ac. Second, we show that KANSL3 protects cells from HU-induced RS. Third, KANSL3 is not involved in replication fork speed or fork protection, but instead supports the restart

of HU-induced stalled replication forks. Finally, KANSL3 suppresses the formation of R-loops. Thus, KANSL3 may ensure fork stability by preventing TRC collisions that are causally linked to R-loop formation and induce replication fork collapse (Fig. 5C).

KANSL3 is dispensable for H4K16Ac and interacts with members of the NSL and MSL complex

The NSL and MSL complex are both MOF containing complexes with distinct functions. On one hand MOF catalyzes H4K16Ac as part of the MSL complex, while on the other hand it promotes cell survival and regulates the transcription of housekeeping genes as part of the NSL complex [19]. However, more recently, disruption of the MSL complex has been linked to H4K16Ac-independent chromosomal instability [29]. In agreement with previous studies we found the NSL complex member KANSL3 to be dispensable for H4K16Ac [20]. Another study reported that KANSL3 may function separately from other NSL and MSL complex members in maintaining the expression of several essential genes and cell survival [19]. Our mass spectrometry experiments revealed that KANSL3 interacts with known members of both the NSL and MSL complex. However, more interestingly, KANSL3 also interacts with subunits of the RNA polymerase II complex (e.g. POLR2A, POLR2B and POLR2E), factors involved in RNA splicing (e.g. SRSF1 and SCAF1) and replisome associated proteins (e.g. SMARCA5) [30] and Table S1). Moreover, KANSL3 was also reported to interact with PCNA upon camptothecin-induced RS [31]. This may suggest that KANSL3 maintains fork integrity: 1) indirectly via H4K16Ac independent transcription regulation, 2) via the suppression of R-loop-associated TRCs due to its interaction with the RNA polymerase II complex and splicing factors, or 3) its interaction with replisome associated proteins. However, further work will be needed to resolve the functional relevance of interplay between KANSL3 and its interaction partners in response to RS.

KANSL3 protects cells from HU-induced replication stress and regulates recovery of stalled replication forks

Our findings show that KANSL3-depleted cells are sensitive to HU-induced RS. We could exclude that the observed sensitivity was due to changes in replication fork speed and/or fork protection. Because HU treatment leads to the formation of stalled replication forks, we asked whether KANSL3 may be involved in their restart. Using EdU incorporation and DNA fiber assays, we confirmed that KANSL3 is implicated in the

restart of HU-stalled replication forks. Interestingly, EdU incorporation was reduced in KANSL3-depleted cells both in unperturbed and RS conditions. This suggests KANSL3 is also involved in normal DNA replication. Given the modest increase in the fraction of G2/M phase cells following KANSL3 depletion, it may be possible that KANSL3-depleted cells suffer from an increase in under-replicated DNA, presumably due to persistent R-loops, which may in turn result in a G2/M arrest, the latter which is in agreement with a previous study [19]. Alternatively, the decrease in EdU incorporation could also be indicative of decreased origin firing. However, further work will be needed to resolve whether KANSL3-depleted cells suffer from increased under-replicated DNA or have a decrease in the number of origins firing.

In response to HU-induced helicase-polymerase uncoupling, ATR kinase is recruited and activated via its direct interaction with ssDNA at stalled replication forks [32]. This is followed by the ATR-dependent phosphorylation of RPA (at Serine 33), which prevents fork breakage by the suppression of new origin firing, thereby preserving the nuclear pool of RPA [3]. Consequently, inhibition of ATR leads to excessive amounts of ssDNA and limits the available amount RPA molecules by a process referred to as 'RPA exhaustion'. This phenomenon in turn leads to replication fork catastrophies and the formation of DSBs [4, 32]. RPA levels, however, remained unaffected in KANSL3-depleted cells, ruling out RPA exhaustion. Instead, we found increased p-RPA (S4/S8) and γ H2AX levels upon RS in KANSL3-depleted cells. This suggests that KANSL3 loss results in the conversion of stalled replication forks into collapsed forks, which may ultimately be converted into DSBs. Given the role of KANSL3 in transcription, the emerging question is whether these events depend on its role in transcription and the formation of R-loop dependent TRCs [33].

KANSL3, but not MOF depletion results in increased R-Loop formation in both HU-treated and untreated conditions

Our data reveal that KANSL3 depletion leads to increased R-loop levels in both unperturbed and RS conditions. However, MOF depletion resulted in reduced R-loops, which is contrary to a previous report [17]. This discrepancy may be explained due to different siRNAs used against MOF in the previous study compared to ours. We used the S9.6 antibody for immunofluorescence (IF) to measure R-loop levels. As expected, we found AQR depletion to increase the formation of R-loops, which validates our S9.6 IF to some extent [34]. However, because S9.6 also recognizes double-strand RNA [28,

35], it is of utmost importance to further validate our S9.6 IF experiments using RnaseIII treatment, treatment with recombinant wildtype human RNaseH1 and its catalytic inactive version, and overexpression of RNaseH1 to further validate the specificity of our S9.6 IF [35].

The unscheduled formation of R-loops has been linked to TRCs and RS [36]. This raises the question whether the aberrant R-loops observed in KANSL3-depleted cells, are a potential mechanism driving RS. Future endeavors including RNaseH1 overexpression rescue experiments in KANSL3-depleted cells will give insight into whether the increase in fork stalling measured by p-RPA (S4/8) and DNA breaks measured by γ H2AX levels, as well as the HU-sensitivity observed in KANSL3-depleted cells is caused by R-loops. Furthermore, R-loops may pose an obstacle for replication fork progression and thereby cause defects in replication fork recovery upon HU-induced RS observed in KANSL3-depleted cells [37]. To investigate this possibility, proximity ligation assay (PLA) between PCNA, as a marker for replication, and RNAPII may evaluate the occurrence of TRCs in absence of KANSL3 [16].

The emerging questions concerning KANSL3's role in R-loops suppression is to decipher the genomic location in which R-loops are enriched. Are they specifically localized at genes regulated by the NSL complex or also at other genes? In depth analysis of R-loop distribution by DRIP-sequencing in both control and KANSL3-depleted cells will be required in the future to address these questions. Depending on the orientation of transcription relatively to the direction of the replication forks, TRCs can occur co-directionally or head-on [36]. Co-directional (CD) collisions can be resolved by displacement of RNA polymerase II from DNA, whereas head-on (HO) collisions induce pausing and blocking of the replication fork and may lead to fork collapse and DSBs [36]. Given that KANSL3-depleted cells display an increase in markers of RS-induced fork collapse (p-RPA (S4/S8) and γ H2AX), it may bind regions in the genome in which HO TRC occur. Future DRIP-seq (R-loops) and ChIP-seq (p-RPA (S4/S8) and γ H2AX) experiments will provide insight into the context in which KANSL3 suppresses R-loop formation and may cause HO collisions [36]. Strikingly, our data revealed that KANSL3 depletion does not only lead to increased R-loops in the nucleus, but also in the cytosol. Cytosolic R-loops are associated with the activation of the innate immune response via the cGAS-STING pathway which regulates the expression of antiviral genes [38]. Future studies will be needed to decipher whether cytosolic R-loops in KANSL3-depleted cells activate the innate immune response and may pave the way for KANSL3's role in anti-tumor immunity [39].

Cooperation of KANSL3 and other NSL complex members

We reveal a critical role for KANSL3 in preventing the formation of R-loops associated RS. However, KANSL3 functions within the NSL-complex and is responsible for the stability and subsequent catalytic activity of the complex via OGT-mediated O-GlcNAcylation of KANSL3 [40]. KANSL1 is the major scaffolding protein within the complex and binds to MOF, PHF20 and MCRC1. Its interaction with MOF determines the catalytic activity of the NSL complex towards H4K16Ac *in vitro* [41]. Importantly, loss of both KANSL2 and KANSL3 is associated with nuclear abnormalities and chromothripsis [20]. Moreover, our KANSL3 interactome data reveals all known NSL-complex members in both unperturbed and RS conditions. Although it remains to be established whether other NSL-complex members are directly involved suppressing R-loop induced RS, these findings suggest that the majority of NSL proteins remain in a complex upon RS. On the one hand, the NSL complex may associate with the replisome via protein-protein interactions with replisome or replisome-associated proteins. On the other hand, given the role of the NSL-complex in transcription regulation and its interaction with members of the RNAPII complex and RNA splicing factors, NSL proteins may regulate the response to RS by controlling R-loop formation. Future mechanistic studies on the NLS protein repertoire will undoubtedly improve our understanding of their crucial role in diverse biological processes, including RS, thereby increasing our understanding of genome stability maintenance.

MATERIAL AND METHODS

Cell lines

U2OS and HCT116 cells were cultured in 5% CO₂ at 37°C in DMEM (Dulbecco's modified Eagle's medium) supplemented with 10% fetal calf serum and antibiotics. HCT116 Flp-In/T-Rex and U2OS Flp-In/T-Rex cells, which were generated using the Flp-In/T-Rex system (Thermo Fisher Scientific), were a gift of Bradley Wouters (Princess Margaret Cancer Centre, Canada) and Geert Kops (University Medical Center Utrecht, the Netherlands). These cells were used to stably express inducible versions of GFP-NLS, as well as siRNA-resistant GFP-KANSL3^{WT} by co-transfection of pCDNA5/FRT/TO-Puro plasmid encoding GFP or GFP-tagged ZNF384 (WT or deletion mutants) (5 µg), together with pOG44 plasmid encoding the Flp recombinase (1 µg). After selection on 1 µg/mL puromycin, single clones were isolated and expanded. Both HCT116 Flp-In/T-Rex clones and U2OS Flp-In/T-Rex were incubated with 2 µg/mL doxycycline for 24h to induce expression of cDNAs. All cells were authenticated by STR profiling and tested negative in routinely performed mycoplasma tests.

Chemicals

Cells were treated with Hydroxyurea (Sigma) at a final concentration of 2 mM or 4 mM for the indicated timepoints and collected for further analysis. The PARP inhibitor olaparib (Selleck Chemicals) was used at a final concentration of 10 μ M.

Transfections, siRNAs and plasmids

Cells were transfected with siRNAs using RNAiMAX (Invitrogen) according to the manufacturer's instructions. Cells were transfected once with siRNAs 24 hours after seeding at a concentration of 20 nM and analyzed 48 hours after transfection unless otherwise indicated. siRNA sequences are listed in Table 1. Cells were transfected with plasmid DNA using Lipofectamine 2000 (Invitrogen) according to the manufacturer's instructions and analyzed 24-48 hours after transfection. The expression vector for full length human KANSL3 (64775; from Addgene; originally from Joan Conaway and Ronald Conaway), was amplified and cloned into pCDNA5/FRT/TO-Puro as a *HindIII/KpnI* fragment (Table 2). siKANSL3-resistant KANSL3 cDNA was generated by introducing the underlined mutations CGACGATAACCTTAGGATCAG by overlap PCR and cloned as *HindIII/KpnI* fragment into pCDNA5/FRT/TO-Puro-KANSL3-WT (Table 2). All KANSL3 expression constructs were verified using Sanger sequencing.

Immunofluorescence analysis

Cells were either directly fixed with 2% formaldehyde in PBS for 20 minutes at room temperature (RT), or pre-extracted with 0.5% Triton-X100 (Serva) in PBS on ice for 2-5 minutes prior to fixation. Alternatively, cells were fixed, post-extracted with 0.25% Triton-X100 (Serva) in PBS and treated with 100 mM glycine in PBS for 20 minutes to block unreacted aldehyde groups. Cells were then rinsed with PBS and equilibrated in wash buffer (PBS containing 0.5% BSA). Antibody incubation steps and washes were in wash buffer. Primary antibodies were incubated for 1-2 hours at room temperature. Detection was done using goat anti-mouse or goat anti-rabbit Ig coupled to Alexa 488, 555 or 647 (1:1500; Invitrogen Molecular probes). All antibodies are listed in Table 3. Samples were incubated with 0.1 μ g/mL 4',6-Diamidino-2-Phenylindole Dihydrochloride (DAPI) and mounted in Polymount.

Sample preparation and mass spectrometry

For mass spectrometry, U2OS Flp-In/T-Rex cells expressing GFP-NLS and GFP-KANSL3^{WT} were treated with 2 mM Hydroxyurea for 4 hours or left untreated. Cell pellets were lysed in EBC-1 buffer (50 mM Tris, pH 7.5, 150 mM NaCl, 0.5% NP-40, 2 mM MgCl₂, protease inhibitor cocktail tablets) with 500 units benzonase. Samples were incubated for 1 hour at 4°C under constant mixing followed by high-speed centrifugation for 10 minutes at 4°C. Protein concentration was measured by Qubit in the cleared lysates, equalized and transferred to tubes containing GFP-Trap beads (Chromotek). After 90 minutes of incubation at 4°C under rotating condition, the beads were washed 4 times with EBC-2 buffer (50 mM Tris pH 7.5, 150 mM NaCl, 1 mM EDTA, and protease inhibitor cocktail tablets) and 3 times with 50 mM ammonium bicarbonate followed by overnight digestion using 2.5 µg trypsin at 37°C under constant shaking. Digestion was terminated with 1% trifluoroacetic acid and centrifuged for 5 minutes at high speed to precipitate insoluble fractions. Consequently, C18 cartridges were prepared by washing 2 times with acetonitrile followed by 2 times with 0.1% Acetic acid. Peptides were loaded on the cartridge, while bound peptides were washed 2 times with 0.1% acetic acid and eluted with 1 mL 80% acetonitrile / 0.1% acetic acid and lyophilized.

Mass spectrometry was performed essentially as previously described [42]. Samples were analysed on a Q-Exactive Orbitrap mass spectrometer (Thermo Scientific, Germany) coupled to an EASY-nanoLC 1000 system (Proxeon, Odense, Denmark). Digested peptides were separated using a 15 cm fused silica capillary (ID: 75 µm, OD: 375 µm, Polymicro Technologies, California, US) in-house packed with 1.9 µm C18-AQ beads (ReproSpher-DE, Pur, Dr. Maisch, Ammerburch-Entringen, Germany). Peptides were separated by liquid chromatography using a gradient from 2% to 95% acetonitrile with 0.1% formic acid at a flow rate of 200 nl/minute for 65 minutes. The mass spectrometer was operated in positive-ion mode at 2.8 kV with the capillary heated to 250°C, and in a Data-Dependent Acquisition (DDA) mode with a top 7 method. Full scan MS spectra were obtained with a resolution of 70,000, a target value of 3×10^6 and a scan range from 400 to 2,000 m/z. Maximum Injection Time (IT) was set to 50 ms. Higher-Collisional Dissociation (HCD) tandem mass spectra (MS/MS) were recorded with a resolution of 35,000, a maximum IT of 20 ms, a target value of 1×10^5 and a normalized collision energy of 25%. The precursor ion masses selected for MS/MS analysis were subsequently dynamically excluded from MS/MS analysis for 60 seconds. Precursor ions with a charge state of 1 and greater than 6 were excluded from triggering MS/MS events. Three replicates were included per condition with two technical repeats each.

Mass spectrometry data analysis

Raw mass spectrometry files were analysed with MaxQuant software (v1.5.3.30) as described [43] with the following modifications from default settings: the maximum number of mis-cleavages by trypsin/p was set to 3, Label Free Quantification (LFQ) was enabled disabling the Fast LFQ feature. Match-between-runs feature was enabled with a match time window of 0.7 minutes and an alignment time window of 20 minutes. We performed the search against an in silico digested UniProt reference proteome for Homo sapiens (8th June 2020). Analysis output from MaxQuant was further processed in the Perseus (v 1.5.5.3) computational platform [43]. Proteins identified as common contaminants, only identified by site and reverse peptide, were filtered out, and then all the LFQ intensities were log₂ transformed. Different biological repeats of each condition were grouped and only protein groups identified in all three biological replicates in at least one condition were included for further analysis. Missing values were imputed using Perseus software by normally distributed values with a 1.8 downshift (log₂) and a randomized 0.3 width (log₂) considering total matrix values. Volcano plots were generated, and Student's T-tests were performed to compare the different conditions. Spreadsheets from the statistical analysis output from Perseus were further processed in Microsoft Excel for comprehensive visualization and analysis of the data (Table S1).

Western blot analysis

Cells were lysed in 2x Laemmli buffer and proteins were separated by Sodium Dodecyl Sulfate PolyAcrylamide Gel Electrophoresis (SDS-PAGE) using 4-12% pre-cast polyacrylamide gels (BioRad or Invitrogen) and MOPS running buffer (Invitrogen). Next, proteins were transferred onto nitrocellulose membranes (Millipore). Protein expression was analyzed by immunoblotting with the indicated primary antibodies (Table 3) and secondary CF680 goat anti-rabbit or CF770 goat anti-mouse Ig antibodies (1:5000, Biotium). Membranes were scanned and analyzed using a Licor Odyssey scanner (LI-COR Biosciences).

Cell survival assays

HCT116 cells were transfected with siRNAs, trypsinized, seeded at low density and exposed to HU for 24 hours. For HCT116 Flp-In/T-Rex, cDNAs were expressed by adding Dox for 24 hours after siRNA transfection. After 12 days, the cells were washed with 0.9% NaCl and stained with methylene blue (2.5 g/L in 5% ethanol, Sigma-Aldrich). Colonies of more than 20 cells were scored.

Cell cycle profiling

Cells were fixed in 70% ethanol, followed by DNA staining with 50 µg/mL propidium iodide in the presence of Rnase A (0.1 mg/mL; Sigma). Cell acquisition and quantification was performed on a BD LSRII flow cytometer (BD Bioscience) using FACSDiva software version 5.0.3.

Chromatin fractionation

Chromatin fractionation was based on a previously published protocol [44] and used with modifications. Briefly, 100.000-150.000 cells were grown per 6-cm dish for 24 h and then transfected with siRNAs. Next, the cells were treated with 500 µM phleomycin for 1 h, washed three times with PBS, and incubated in NETN extraction buffer (100mM NaCl, 1mM EDTA, 20mM Tris-Cl pH8, 0,5% NP-40 + Proteasome inhibitors). After 15 minutes of incubation on ice, samples were taken for the chromatin-unbound fraction and mixed with the same amount of 2x Laemmli buffer. Cells were washed with PBS, lysed, and incubated in Laemmli buffer with benzonase for 15 min to obtain the chromatin-bound fraction. Samples were heated for 7 min at 80°C and subjected to Western blot analysis.

DNA fiber assays

DNA fibers were prepared as described previously [45] with minor modifications. Briefly, siRNA transfected U2OS cells were pulse labelled with 10 µM 5-chloro-2-deoxyuridine (CldU) for 20 min, followed by 250 µM 5-iodide-2-deoxyuridine (IdU) chase for 20 min. Next, cells were washed twice with PBS, trypsinized and resuspended in PBS containing 10% FBS. 5 µl Cell suspension was spotted on the top of a Superfrost glass slide (Fisher Scientific) and dried for 5 min. Subsequently, 7 µl lysis buffer (200 mM Tris-HCl [pH 7.4]; 50 mM EDTA; 0.5% SDS) was added in the middle of the cell suspension, mixed by stirring and incubated for 3 min. Slides were tilted slightly at an angle to induce slow running of a stream of DNA down the slide, air dried, and fixed in methanol:acetic acid (3:1) for 10 min. DNA fibers were denatured with 2.5 M HCl for 80 min, washed three times with PBS and blocked twice with TPB (1% BSA in PBS with 0.1% Tween) for 15 min. Labelled DNA fibers were then stained with rat anti-BrdU antibody (Clone Bu1/75; for CldU detection; Abcam) and mouse anti-BrdU antibody (clone B44; for IdU detection; Abcam) in TPB for 1 hr at room temperature. After incubation, slides were washed thrice with PBS and three times with TPB, followed by fixation in 2% formaldehyde for 10 min.

The microscope slides were then incubated with Alexa Fluor 488 donkey anti-rat antibody (1:1000) and Alexa Fluor 555 goat anti-mouse antibody (1:1000) in TPB for 1.5 hr at room temperature in the dark. Next, the slides were washed three times with PBS, air-dried and mounted with aqua polymount (Polysciences). Fluorescent images were acquired, and track lengths were measured manually using ImageJ software. For fork degradation, cells were incubated with 20 μM CldU for 20 min, followed by 25 μM IdU chase for 20 min, and finally 4 mM hydroxyurea treatment for 5 hr, before trypsinization and slide preparation as described above. For fork recovery, cells were labelled with 20 μM CldU for 20 min, followed by 4 mM hydroxyurea treatment for 5 hr, and finally 250 μM IdU labelling.

EdU incorporation assay

U2OS cells were transfected with siRNAs and 48 hours later left untreated or treated with 2 mM HU for 2 hours. After washing, the cells were further incubated in medium containing 5-ethynyl-2'-deoxyuridine (EdU) for 15 min, 60 min, 90 min and 2 hours and pre-extracted with 0.5% ice-cold Triton-X-100 (Serva) in PBS and fixed with 2% formaldehyde in PBS for 20 minutes at room temperature (RT). Next, cells were permeabilized with 0.25% Triton X-100 in PBS for 5 min at room temperature, followed by incubation with click-iT reaction buffer (10 μM biotin azide (life technologies), 10 mM sodium-L-ascorbate, and 2 mM CuSO_4) for 30 min in at RT. Cells were then rinsed with PBS and equilibrated in wash buffer (PBS containing 0.5% BSA. Samples were incubated with 0.1 $\mu\text{g}/\text{mL}$ 4',6-Diamidino-2-Phenylindole Dihydrochloride (DAPI) and mounted in Polymount.

AUTHOR CONTRIBUTIONS

J.S. performed western blot analysis, immunofluorescence experiments, clonogenic survival assays. J.L. and W.W.W. performed DNA fiber assay. A.J.L.G. prepared mass-spectrometry samples. R.P. and A.C.O.V. performed mass-spectrometry experiments and data analysis. H.v.A. conceived and supervised the project.

ACKNOWLEDGEMENTS

We thank Niels Mailand for kindly providing valuable reagents. This research was financially supported by the European Research Council (ERC) under the European Union's Horizon 2020 research and innovation program (ERC-StG 310913 to A.C.O.V.; ERC-CoG 50364 to H.v.A)

REFERENCES

1. Gaillard, H., T. García-Muse, and A. Aguilera, *Replication stress and cancer*. Nature Reviews Cancer, 2015. **15**(5): p. 276-289.
2. Zeman, M.K. and K.A. Cimprich, *Causes and consequences of replication stress*. Nat Cell Biol, 2014. **16**(1): p. 2-9.
3. Toledo, L.I., et al., *ATR prohibits replication catastrophe by preventing global exhaustion of RPA*. Cell, 2013. **155**(5): p. 1088-103.
4. Haahr, P., et al., *Activation of the ATR kinase by the RPA-binding protein ETAA1*. Nature Cell Biology, 2016. **18**(11): p. 1196-1207.
5. Bass, T.E., et al., *ETAA1 acts at stalled replication forks to maintain genome integrity*. Nat Cell Biol, 2016. **18**(11): p. 1185-1195.
6. Zhao, H. and H. Piwnica-Worms, *ATR-mediated checkpoint pathways regulate phosphorylation and activation of human Chk1*. Molecular and cellular biology, 2001. **21**(13): p. 4129-4139.
7. Neelsen, K.J. and M. Lopes, *Replication fork reversal in eukaryotes: from dead end to dynamic response*. Nature Reviews Molecular Cell Biology, 2015. **16**(4): p. 207-220.
8. Liao, H., et al., *Mechanisms for stalled replication fork stabilization: new targets for synthetic lethality strategies in cancer treatments*. EMBO Rep, 2018. **19**(9).
9. Schlacher, K., H. Wu, and M. Jasin, *A distinct replication fork protection pathway connects Fanconi anemia tumor suppressors to RAD51-BRCA1/2*. Cancer Cell, 2012. **22**(1): p. 106-16.
10. Quinet, A., et al., *To skip or not to skip: choosing repriming to tolerate DNA damage*. Molecular Cell, 2021. **81**(4): p. 649-658.
11. Lin, Y.-L. and P. Pasero, *Transcription-Replication Conflicts: Orientation Matters*. Cell, 2017. **170**(4): p. 603-604.
12. Nguyen, H.D., et al., *Functions of Replication Protein A as a Sensor of R Loops and a Regulator of RNaseH1*. Mol Cell, 2017. **65**(5): p. 832-847.e4.
13. Gaillard, H. and A. Aguilera, *Transcription as a Threat to Genome Integrity*. Annu Rev Biochem, 2016. **85**: p. 291-317.
14. Crossley, M.P., M. Bocek, and K.A. Cimprich, *R-Loops as Cellular Regulators and Genomic Threats*. Mol Cell, 2019. **73**(3): p. 398-411.
15. Rinaldi, C., et al., *Sensing R-Loop-Associated DNA Damage to Safeguard Genome Stability*. Frontiers in Cell and Developmental Biology, 2021. **8**(1657).
16. Bayona-Feliu, A., et al., *The SWI/SNF chromatin remodeling complex helps resolve R-loop-mediated transcription-replication conflicts*. Nature Genetics, 2021.
17. Singh, D.K., et al., *MOF Suppresses Replication Stress and Contributes to Resolution of Stalled Replication Forks*. Mol Cell Biol, 2018. **38**(6).
18. Sheikh, B.N., S. Guhathakurta, and A. Akhtar, *The non-specific lethal (NSL) complex at the crossroads of transcriptional control and cellular homeostasis*. EMBO Rep, 2019. **20**(7): p. e47630.
19. Radzishenskaya, A., et al., *Complex-dependent histone acetyltransferase activity of KAT8 determines its role in transcription and cellular homeostasis*. Mol Cell, 2021. **81**(8): p. 1749-1765.e8.
20. Karoutas, A., et al., *The NSL complex maintains nuclear architecture stability via lamin A/C acetylation*. Nature Cell Biology, 2019. **21**(10): p. 1248-1260.

21. Ronson, G.E., et al., *PARP1 and PARP2 stabilise replication forks at base excision repair intermediates through Fbh1-dependent Rad51 regulation*. Nature Communications, 2018. **9**(1): p. 746.
22. Maya-Mendoza, A., et al., *High speed of fork progression induces DNA replication stress and genomic instability*. Nature, 2018. **559**(7713): p. 279-284.
23. Mijic, S., et al., *Replication fork reversal triggers fork degradation in BRCA2-defective cells*. Nature Communications, 2017. **8**(1): p. 859.
24. Iyer, D.R. and N. Rhind, *Replication fork slowing and stalling are distinct, checkpoint-independent consequences of replicating damaged DNA*. PLoS Genet, 2017. **13**(8): p. e1006958.
25. Petermann, E., et al., *Hydroxyurea-Stalled Replication Forks Become Progressively Inactivated and Require Two Different RAD51-Mediated Pathways for Restart and Repair*. Molecular Cell, 2010. **37**(4): p. 492-502.
26. Lam, K.C., et al., *The NSL complex-mediated nucleosome landscape is required to maintain transcription fidelity and suppression of transcription noise*. Genes Dev, 2019. **33**(7-8): p. 452-465.
27. Crossley, M.P., et al., *Catalytically inactive, purified RNase H1: A specific and sensitive probe for RNA-DNA hybrid imaging*. J Cell Biol, 2021. **220**(9).
28. Sollier, J., et al., *Transcription-Coupled Nucleotide Excision Repair Factors Promote R-Loop-Induced Genome Instability*. Molecular Cell, 2014. **56**(6): p. 777-785.
29. Monserrat, J., et al., *Disruption of the MSL complex inhibits tumour maintenance by exacerbating chromosomal instability*. Nature Cell Biology, 2021. **23**(4): p. 401-412.
30. Ribeyre, C., et al., *Nascent DNA Proteomics Reveals a Chromatin Remodeler Required for Topoisomerase I Loading at Replication Forks*. Cell Reports, 2016. **15**(2): p. 300-309.
31. Srivastava, M., et al., *Replisome Dynamics and Their Functional Relevance upon DNA Damage through the PCNA Interactome*. Cell Reports, 2018. **25**(13): p. 3869-3883.e4.
32. Liao, H., et al., *Mechanisms for stalled replication fork stabilization: new targets for synthetic lethality strategies in cancer treatments*. EMBO reports, 2018. **19**(9): p. e46263.
33. Gaub, A., et al., *Evolutionary conserved NSL complex/BRD4 axis controls transcription activation via histone acetylation*. Nature Communications, 2020. **11**(1): p. 2243.
34. Sakasai, R., et al., *Aquarius is required for proper CtIP expression and homologous recombination repair*. Scientific Reports, 2017. **7**(1): p. 13808.
35. Crossley, M.P., et al., *Catalytically inactive, purified RNase H1: A specific and sensitive probe for RNA-DNA hybrid imaging*. Journal of Cell Biology, 2021. **220**(9).
36. García-Muse, T. and A. Aguilera, *Transcription-replication conflicts: how they occur and how they are resolved*. Nature Reviews Molecular Cell Biology, 2016. **17**(9): p. 553-563.
37. Gómez-González, B. and A. Aguilera, *Transcription-mediated replication hindrance: a major driver of genome instability*. Genes Dev, 2019. **33**(15-16): p. 1008-1026.
38. Mankan, A.K., et al., *Cytosolic RNA:DNA hybrids activate the cGAS-STING axis*. Embo j, 2014. **33**(24): p. 2937-46.
39. Li, T. and Z.J. Chen, *The cGAS-cGAMP-STING pathway connects DNA damage to inflammation, senescence, and cancer*. Journal of Experimental Medicine, 2018. **215**(5): p. 1287-1299.
40. Wu, D., et al., *O-Linked N-acetylglucosamine transferase 1 regulates global histone H4 acetylation via stabilization of the nonspecific lethal protein NSL3*. J Biol Chem, 2017. **292**(24): p. 10014-10025.

41. Li, X., et al., *Two mammalian MOF complexes regulate transcription activation by distinct mechanisms*. Mol Cell, 2009. **36**(2): p. 290-301.
42. Kumar, R., et al., *The STUbL RNF4 regulates protein group SUMOylation by targeting the SUMO conjugation machinery*. Nat Commun, 2017. **8**(1): p. 1809.
43. Tyanova, S., T. Temu, and J. Cox, *The MaxQuant computational platform for mass spectrometry-based shotgun proteomics*. Nat Protoc, 2016. **11**(12): p. 2301-2319.
44. Feng, W., et al., *TRAIIP regulates replication fork recovery and progression via PCNA*. Cell Discov, 2016. **2**: p. 16016.
45. Nieminuszczy, J., R.A. Schwab, and W. Niedzwiedz, *The DNA fibre technique - tracking helicases at work*. Methods, 2016. **108**: p. 92-8.

Table 1. List of siRNAs

Target	Sequence (5'-3')
MOF	GUGAUCCAGUCUCGAGUGAUU
KANSL3	UGAUGACAAUCUCAGAAUA
RAD51	GAGCUUGACAAACUACUUC
BRCA2	GAAGAAUGCAGGUUUAUA
ETAA1	GAGCAAAACAAGAGGAAUUUU
Luciferase	CGUACGCGGAUACUUCGA
AQR	SMARTpool (siGENOME)

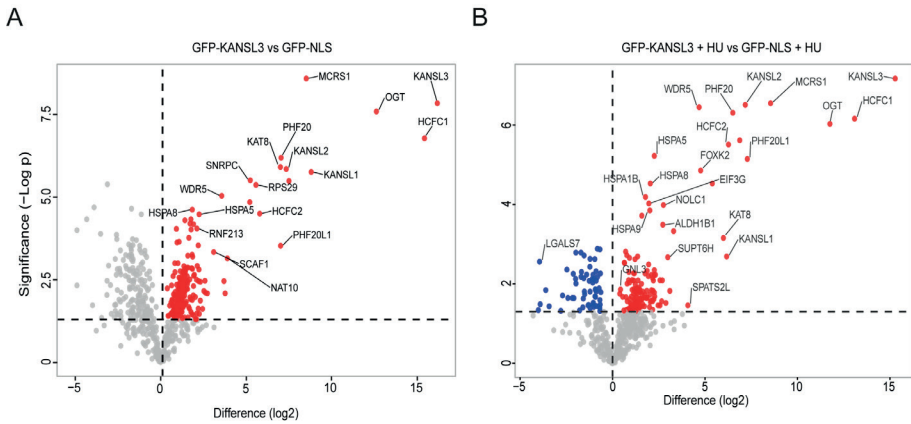
Table 2. List of primers

Name	Sequence (5'-3')
HindIII FW	TAAAAAGCTTATATGGAAGAATCTCACTTCAATTCTAAC
KpnI RV	TAATAATGGTACCCTAAGAGCTGGCCAGGTGC
KANSL3_siRNAres_HindII Rv	TAATAATGGTACCTCAGGGTGCTGGAGGC
KANSL3_siRNAres_KpnI FW	TAAAAAGCTTATATGGCCCACCGGGGTGG
M13 FW	GTAAAACGACGGCCAGT
M13 RV	CAGGAAACAGCTATGAC

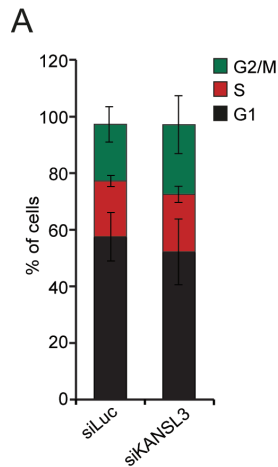
Table 3. List of primary antibodies

Protein	Host	Company	IF	WB
GFP	Mouse	Roche (11814460001)		1:1000
α -Tubulin	Mouse	Sigma (cloneDM1A, T6199)		1:5000
KANSL3	Rabbit	ATLAS (HPA030358)		1:2000
RAD51	Rabbit	BioAcademia		1:15000
H4K16Ac	Rabbit	Active Motif (39930)		1:2000
MOF	Rabbit	Bethyl Laboratories		1:1000
H4	Mouse	Abcam (ab31810)		1:2000
p-RPA (S4/S8)	Rabbit	Bethyl Laboratories (A300-245A)	1:1000	1:1000
ETAA1	Rabbit	Kind gift of Niels Mailand		1:400
RPA	Mouse	Abcam (ab2175)	1:1000	1:1000

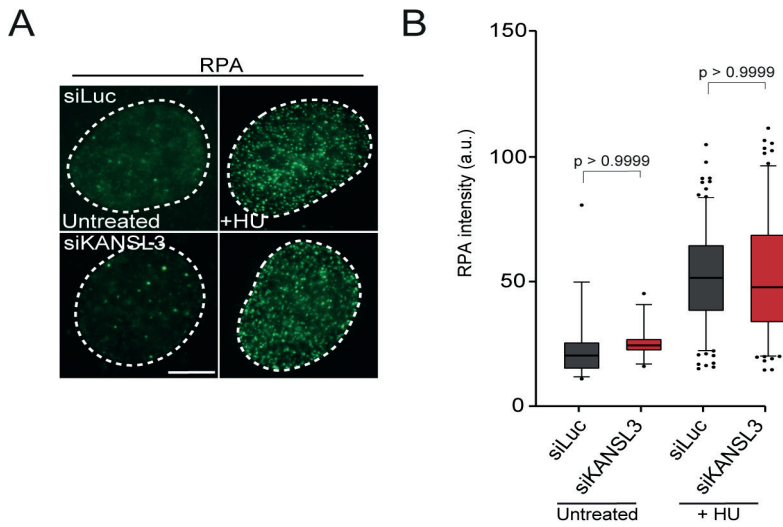
SUPPLEMENTARY FIGURES AND TABLES



Supplementary Figure 1. – related to Figure 1. KANSL3 interacts with members of the MSL and NSL complex. (A) Volcano plot depicting the statistical differences of the MS analysis on GFP-KANSL3 versus GFP-NLS pull-downs. The enrichment is plotted on the x-axis and the significance (t-test $-\log_2$ p-value) is plotted on the y-axis (see also Supplementary Table 1). (B) As in A, except that cells were treated with 2 mM HU for 4 hours before pull-downs.



Supplementary Figure 2. – related to Figure 2. Cell cycle profiles remain unaffected in KANSL3-depleted cells. (A) Cell cycle profile of the indicated siRNA-transfected knockdown U2OS cells. The fraction of G1-, S- and G2-phase cells was determined by propidium iodide staining and FACS analysis.



Supplementary Figure 3. – related to Figure 3. RPA foci intensity remains unaffected in KANSL3-depleted cells. (A) Cell cycle profile of the indicated siRNA-transfected knockdown U2OS cells. The fraction of G1-, S- and G2-phase cells was determined by propidium iodide staining and FACS analysis. (B) RPA foci formation in U2OS cells transfected with the indicated siRNAs. Cells were exposed to 2 mM of HU and foci intensity was measured after 4 hours. (F) Quantification of RPA foci intensity in cells from A. Mean foci intensity was quantified in immunostained RPA cells.

KANS3 suppresses R-loop formation and replication fork instability

Table with 4 columns: Gene Name, Gene ID, Start, End, Orientation, and RefSeq ID. The table lists numerous genes and their genomic coordinates on chromosomes 1 through 22.

4

